

Synthesis of nanostructured composite materials of MoO₃/TiO₂–SiO₂ with spherical shape prepared with resins

S. A. Kuznetsova¹, O. S. Khalipova¹, K. V. Lisitsa¹, A. A. Ditts², A. G. Malchik², V. V. Kozik¹

¹National Research Tomsk State University, Lenin, 36, Tomsk, 634050 Russia

²National Research Tomsk Polytechnic University, Lenin, 30, Tomsk, 634050 Russia

onm@mail.tsu.ru

DOI 10.17586/2220-8054-2021-12-2-232-245

The aim of this work was to synthesize of nanostructured MoO₃/TiO₂–SiO₂ composites with hollow spherical shape by thermal decomposition of anion exchangers saturated with Mo₇O₂₄⁶⁻ ions and treated with the TBT–TEOS sol. The effect of the kinetics (Kissinger and the Metzger–Horowitz methods) of thermal decomposition of resins of porous and gel structures on the size of MoO₃ nanoparticles and the strength of MoO₃/TiO₂–SiO₂ spheres was shown. The formation of dense spherical nanostructured agglomerates of the composite is facilitated by reactions occurring at the interface between the phases of cylindrical and spherical symmetry when using an anion exchange resin with a porous structure. The decomposition reactions of the anion-exchange resin of the gel structure, accompanied by random nucleation, lead to the formation of hollow spherical agglomerates of the composite with cracks on the surface. The materials were characterized by DSC–TGA, XRD and SEM.

Keywords: MoO₃/TiO₂–SiO₂; metal oxide; anion-exchange resin; decomposition; hollow sphere.

Received: 18 February 2021

Revised: 19 March 2021

1. Introduction

Hollow spheres of metal oxides are intensively investigated for applications, such as controlled release capsules for drugs, fillers, filters [1], gas sensitive materials [1, 2], absorbents and separation materials, especially for fixed-bed reactors or chromatography columns [3]. In recent years, hollow spheres of metal oxides have also been intensively investigated for applications as catalysts [3–7]. This is because metal oxide with hollow micro and nanospheres only has low density and good porous structure (usually contain both mesopores and macropores [3]), but also provides a high surface area with more active acid-base oxide centers on the pore surface [4].

Many approaches to the preparation of oxide materials with spherical form of agglomerates have been proposed to date, such as emulsion approaches [8], spray pyrolysis techniques [2], and templating synthesis [1]. Among these numerous techniques of hollow spheres production, thermal decomposition of ion-exchange resins loaded with the metal ions is the most attractive one due to its simplicity, ease for scale-up (in industry), and high quality resulting materials [1, 4, 5]. In addition, templates and precursors are all commercially available and inexpensive. Moreover, it has been reported [4] that using ion-exchange resin as a template can promote the formation of crystalline framework with high structural stability in spherical agglomerates that can endure high temperature and other rigorous conditions. This method was used for the first time for preparing plutonium oxide microspheres as early as 1989 [9]. Later it was successfully applied to obtain spherical particles of Fe₂O₃ [3, 10], porous Al₂O₃, TiO₂ [3] and ZrO₂/Al₂O₃ macrobeads [4], MoO₃ microspheres [1] and TiO₂–SiO₂/M_xO_y (M = Co, Cr) [6] and MoO₃–TiO₂–SiO₂ composites [5]. Resins with various compositions and structures were used in these studies. Wang et al. [3] have reported a method of preparing Fe₂O₃, Al₂O₃, TiO₂ macrobeads using a cation-exchange resin with sulfonic acid groups as templates and aqueous solutions of metal salts as precursors. In a follow-up work, Wang et al. [4] have reported a method to prepare porous ZrO₂ and ZrO₂/Al₂O₃ macrobeads using cation exchange resins with sulfonate groups as templates (D72 in H⁺ – type, poly (styrene-co-divinylbenzene) – matrix). Wang et al. [3] have shown that the loading content of metal ions plays a key role in the preparation of metal oxide macrobeads with uniformity and integrity. Li et al. [1] have successfully prepared hollow MoO₃ microspheres by using anion exchange resin spheres Dowex 2 (Sigma Company) in carbonated form and 12-molybdodiphosphoric acid solution (1 M, H₃PMo₁₂O₄₀) as precursors. In their work [1], it was shown that the choosing of appropriate calcination temperature is important to obtain hollow spheres. If the temperature was increased to above 650 °C, no hollow spheres but white needle crystals form. In addition, they reported that the heating temperature should not be raised too rapidly, otherwise the gas resulting from the organic resin decomposition and oxidation created pressure which broke the sphere shells.

Despite numerous studies, there is no explanation which allows us to obtain strong spheres of oxide composites by the thermal decomposition of ion-exchange resins. It is still an urgent problem to select an ion-exchange resin, which allows one to obtain agglomerates with strong spherical form. We believe that the formation of strong spherical

agglomerates is primarily influenced by the mechanism of thermal destruction of the ion-exchange resin. In a previous study [5], we demonstrated a route to prepare spherical particles of $\text{MoO}_3\text{-TiO}_2\text{-SiO}_2$ composites using TOKEM-400 and TOKEM-840 anion-exchange resins of the gel structure. It was established that the resin type influenced the surface morphology of the composites. Materials based on molybdenum(VI) and titanium(IV) oxides are very important because of their wide applications in gas sensors, solar cells, supercapacitors; electrochromic and photochromic materials, and catalysts [11–18]. Silicon (IV) oxide was chosen as a binder for the formation of mechanically strong spheres. Although several efforts have been reported to study the kinetics of the thermal decomposition of ion-exchange resins [19, 20], the study on spheres formation as a result of thermal decomposition of ion-exchange resins preliminarily loaded with the metal ions is still limited. The scientific literature contains information on molybdenum-containing polymer-salt precursors, which shows the effect of the polymer composition on their thermal stability and properties of the obtained oxide compositions based on molybdenum oxides [21–23].

The aim of this study was to determine how the decomposition kinetics of anion-exchange resins TOKEM-320Y and TOKEM-400 influences the formation of the $\text{MoO}_3/\text{TiO}_2\text{-SiO}_2$ nanocomposites with spherical shape of agglomerates. The detailed analysis of thermal decomposition of anion-exchange resins preliminarily loaded with the $\text{Mo}_7\text{O}_{24}^{6-}$ ions with the applied $\text{Ti}(\text{C}_4\text{H}_9\text{O})_4 - \text{Si}(\text{C}_2\text{H}_5\text{O})_4 - \text{C}_4\text{H}_9\text{OH}$ sol and structural and morphological characteristics of prepared nanocomposites was carried out. The kinetics of the thermal decomposition of resins in hydroxyl form were also studied in the same conditions.

2. Experimental

2.1. Preparation of composites

The preparation of composites based on $\text{MoO}_3/\text{TiO}_2\text{-SiO}_2$ with spherical shape of agglomerates was done according to the procedure, which was proposed in our previous works [5, 7]. In the first step, TOKEM-320Y and TOKEM-400 anion-exchange resins preliminarily loaded with $\text{Mo}_7\text{O}_{24}^{6-}$ ions were prepared. Weakly basic anion exchangers consisting of the styrene–divinylbenzene matrix (TOKEM-320Y) and polyacrylate matrix (TOKEM-400) with tertiary amine in the hydroxyl form manufactured by PO Tokem (Kemerovo, Russia) were used as organic matrices. These resins consist of spherical granules of 0.40–1.25 mm size. The anion exchangers were placed in a saturated aqueous solution of $(\text{NH}_4)_6\text{Mo}_7\text{O}_{24}\cdot 4\text{H}_2\text{O}$ (0.24 M) (Yugraktiv, Russia) at room temperature for 24 h with continuous stirring on a magnetic stirrer. The resins were then filtered off, washed with a small amount of water, and dried at 60°C to constant weight in air. The synthesized samples were designated as $\text{Mo}_7\text{O}_{24}^{6-}$ (320Y) and $\text{Mo}_7\text{O}_{24}^{6-}$ (400).

In the second step, the dried resins loaded with $\text{Mo}_7\text{O}_{24}^{6-}$ ions were placed in the sol based on tetrabutoxytitanium (TBT, Acros, USA) and tetraethoxysilane (TEOS, Ecos-1, Russia). The aggregatively stable sol was prepared in accordance with a procedure proposed earlier by Shamsutdinova et al. [24, 25]. The mixture of TBT and TEOS was dissolved in a solution consisting of $\text{C}_4\text{H}_9\text{OH}$ (Ecos-1, Russia), H_2O and HNO_3 . The solute concentrations of TBT, TEOS and HNO_3 were 0.1; $2.2\cdot 10^{-2}$ and $2.5\cdot 10^{-3}$ mol L^{-1} respectively (initial HNO_3 concentration was 70 wt. %). The composition was selected based on the earlier study [5]. The sol was kept at room temperature for 3 days. After applying the sol onto the prepared $\text{Mo}_7\text{O}_{24}^{6-}$ (320Y) and $\text{Mo}_7\text{O}_{24}^{6-}$ (400) samples, they were dried at 60°C to constant weight. The samples were denoted as TBT–TEOS/ $\text{Mo}_7\text{O}_{24}^{6-}$ (320Y) and TBT–TEOS/ $\text{Mo}_7\text{O}_{24}^{6-}$ (400).

At the last stage, the dried samples were annealed at 350°C for 6 h and at 500°C for 5 h. The heating rate of the muffle furnace was 14 deg min^{-1} . The $\text{MoO}_3/\text{TiO}_2\text{-SiO}_2$ composites with spherical shape of agglomerates were formed and denoted as $\text{MoO}_3/\text{TiO}_2\text{-SiO}_2$ (320Y) and $\text{MoO}_3/\text{TiO}_2\text{-SiO}_2$ (400).

2.2. Characterization

The working range of pH of the TOKEM-320Y and TOKEM-400 resins in which they exhibit the maximal exchange capacity was determined by potentiometric titration [26]. Potentiometric titration was performed by the method of individual batches. The series of 0.1 g portions of the resins in the OH form were placed in glass flasks (volume 50 mL) with glass stopper and poured of the HCl with various concentrations. The ionic strength of solution was kept at 0.1 by adding NaCl. The total solution volume was 20 mL. The range of acid concentrations was from 0 to 12 mmol g^{-1} ($C_{init} = 0.1$ mol L^{-1}). After the equilibrium was attained (24 h), the pH value of the equilibrium solutions was measured with an I-160 MI pH meter (ESK-1062 combined glass electrode). The titration curve in the pH–titrant amount (HCl, mmol g^{-1} resin) coordinates was obtained.

The total static ion exchange capacity was determined as described in our previously work [5]. Portions (0.1 g) of the air-dry resin (TOKEM-320Y or TOKEM-400) in the OH form were placed in Erlenmeyer flasks, poured over with 25 mL of 0.1 mol L^{-1} HCl, and left for a week to attain the equilibrium. The solution was then separated from the resin, and the decrease in the HCl concentration was determined by titration with 0.1 mol L^{-1} NaOH in the presence

of the mixed indicator until the green color of the solution changed to pink. The total ion exchange capacity (TEC, mmol g⁻¹ resin) was calculated by the equation:

$$TEC = \frac{(c_0 - c_1) V \cdot 100}{m (100 - W)}, \quad (1)$$

where c_0 is the initial HCl concentration (mol L⁻¹); c_1 is the HCl concentration after attaining the equilibrium (mmol L⁻¹); V is the HCl solution volume (L); m is the weight of the air-dry resin portion (g); and W is the weight fraction of moisture in the resin.

The determination of moisture content was carried out experimentally. A portion of the air-dry ion-exchange resin in the OH form was weighed and placed in a weighing bottle preliminarily dried to constant weight. The weighing bottle with sample was weighed, placed in an oven and dried at 100°C to constant weight. Then, the weighing bottle was allowed to cool to room temperature and weighed again. Before and after drying the weighing bottle with a resin was weighed on an analytical balance with an accuracy of 0.0001 g. The weight fraction of moisture in the resin ($W\%$) was defined as follows:

$$W = \frac{(m_1 - m_2)}{m_1} \cdot 100, \quad (2)$$

where m_1 and m_2 are the weights of the swollen and dry resin (g), respectively.

The Mo₇O₂₄⁶⁻ concentration in the initial and equilibrium solutions after the sorption was determined gravimetrically [5, 27] by precipitation of Mo₇O₂₄⁶⁻ ions in the form of PbMoO₄.

The main stages of composites formation and the temperature conditions of the samples annealing were chosen on the basis of thermal analysis of TOKEM-320Y, TOKEM-400 and anion-exchange resins preliminarily loaded with Mo₇O₂₄⁶⁻ ions and treated with the Ti(C₄H₉O)₄ – Si(C₂H₅O)₄ – C₄H₉OH sol. Synchronous thermal analysis was conducted using an STA 449 F1 Jupiter thermoanalyzer interfaced with a QMS 403 Aolos gas mass spectrometer (Netzsch-Gertebau GmbH, Germany). The samples were heated in air in the temperature interval from 25 to 1000°C and a heating rate of 7, 10, and 12 deg min⁻¹, respectively. The measurements for each sample were conducted twice. The kinetic parameters of the decomposition of anion exchangers were established by using Kissinger and Metzger-Horowitz methods. According to the Kissinger method [28–31], at a constant rate of heating of a solid substance, the maximum decomposition rate (β) of a substance is achieved at temperature (T_{\max}), which is related by the equation:

$$\frac{d\left(\ln \frac{\beta}{T_{\max}^2}\right)}{d\left(\frac{1}{T_{\max}}\right)} = -\frac{E}{R} \quad (3)$$

Therefore, the activation energy can be calculated from the slope of the line between $\ln\left(\frac{\beta}{T_{\max}^2}\right)$ and $\frac{1}{T_{\max}}$. In equation (3), the activation energy is independent of the order of the reaction. The reaction order (n) can be calculated from shape index (S) of endothermic or exothermic peaks (Fig. 1) as follows:

$$n = 1.26 \cdot S^{0.5}, \quad (4)$$

$$S = \frac{a}{b}. \quad (5)$$

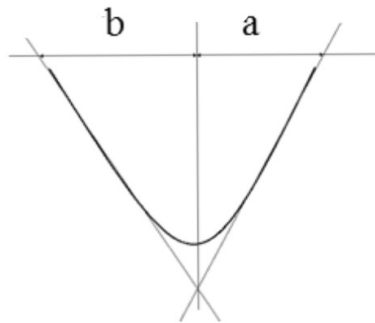


FIG. 1. Shape index for typical endothermic DSC peak

TABLE 1. The properties of TOKEM-400 and TOKEM-320Y anion-exchange resins

Resin	SC ±0.06, mmol-equiv g ⁻¹	TEC ±0.2, mmol-equiv g ⁻¹	W ±0.3, %
TOKEM-400	6.64	9.2	29.1
TOKEM-320Y	1.97	7.2	51.0

The activation energy can be calculated by the Metzger-Horowitz method [32]. The Metzger-Horowitz equation is as follows:

$$\frac{(1-\alpha)^{1-n}-1}{1-n} = -\frac{RT_{\max}^2}{Ea} \exp\left[-\frac{Ea}{RT}\left(1-\frac{\Theta}{T_{\max}}\right)\right], \quad (6)$$

where Θ – the difference between the maximum temperature and the current temperature, α – degree of conversion.

If the reaction order is known, one can determine the activation energy from the angle of the straight line, obtained in a graphical dependence $\frac{(1-\alpha)^{1-n}-1}{1-n}$ on Θ . When $\Theta = 0$, that is, if the decomposition reaction rate reaches a maximum, then $(1-\alpha_{\max}) = n^{1/(1-n)}$. The reaction order determined by the Kissinger method was used to calculate the activation energy by the Metzger-Horowitz method. The kinetic equation for each stage of decomposition of the sample was selected by the Shatava method [33]. The linearity of the function $\log(\alpha)$ versus $\frac{1}{T}$ for the selected kinetic equation on the linearity segment of the dependence of $-\log(\alpha)$ on $\frac{1}{T}$ was checked by trial and error. Of the several kinetic equations tested, one was selected for which the correlation coefficient was maximum.

The phase composition of the samples was determined by X-ray diffraction (XRD) using a Rigaku Miniflex 600 diffractometer (Rigaku, Japan) with CuK α radiation in the 2θ range 10° to 80°. The diffraction pattern was scanned by steps of 0.02° and recording rate of 2 deg min⁻¹. Resulting diffractograms were interpreted with JCPDS-ICDD diffraction database. The MoO₃ structure was refined by the Rietveld method by using the ReX powder diffraction program [34, 35]; the crystal structure model was constructed using the VESTA program [36].

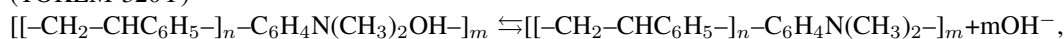
The morphology of the samples was studied by scanning electron microscopy (SEM). The distribution of the elements on the surface was determined on the basis of energy-dispersive X-ray spectroscopic (EDS) analysis. It was performed on a Hitachi TM-3000 scanning electron microscope with a ShiftED 3000 electron microprobe (Hitachi High-Technologies Corporation, Japan).

3. Results and discussion

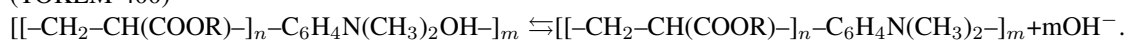
3.1. Properties of anion-exchangers

TOKEM-320Y and TOKEM-400 anion-exchangers have different structures and compositions. TOKEM-320Y is a weakly basic anion-exchange resin of porous structure with the styrene-divinylbenzene matrix and tertiary amine functional groups. TOKEM-400 is a weakly basic non-porous anion-exchange resin of gel structure with a polyacrylate matrix and tertiary amino functional groups. These resins are free bases that undergo dissociation in an aqueous solution as follows:

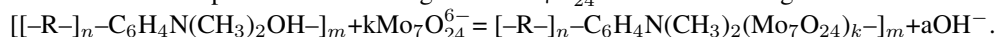
(TOKEM-320Y)



(TOKEM-400)



These resins are capable of ion exchange with Mo₇O₂₄⁶⁻. The ion exchange reaction can be expressed as follow:



The titration curves of anion-exchange resins are shown in Fig. 2.

One single pH drop on the titration curves indicates that the resins are monofunctional. The titration curves exhibit no ascents throughout the examined pH interval. This infers that there are no intramolecular interactions of the functional groups. The equivalence points coincide and correspond to a pH value of 4.6 for TOKEM-400 and TOKEM-320Y. Hence, the maximum exchange capacity of anion-exchange resins is realized at pH < 4.6. The pH of a saturated aqueous solution of ammonium paramolybdate corresponds to a value of 6.79 ± 0.03, which is within the working interval of the maximal capacity of the above anion-exchangers resins. The properties of the resins (sorption capacity of SC, total exchange capacity of TEC and moisture absorption W) are presented in Table 1.

The sorption capacity of the TOKEM-400 and TOKEM-320Y resins with respect to Mo₇O₂₄⁶⁻ is less than the exchange capacity. This indicates that not all the OH⁻ groups of the resins participate in the exchange reaction. This

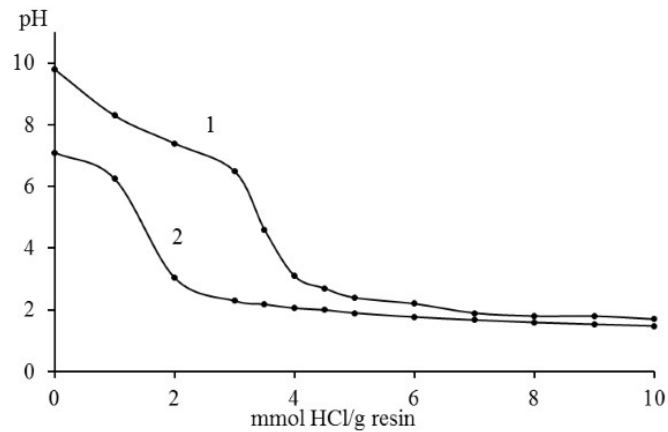


FIG. 2. Titration curves of OH forms of anion-exchange resins with HCl solution: (1) TOKEM-400 and (2) TOKEM-320Y

fact can be explained by an increase in the rigidity of the polymer framework from the surface to the center of the resin grain in swelling in the saturated solution and a decrease in the size of the voids between polymer chains, which leads to a decrease in the cell size between the chains of the polymer preventing penetration of bulky $\text{Mo}_7\text{O}_{24}^{6-}$ ions into the exchange sites.

The differential thermogravimetric (DTG) and thermogravimetric (TG) curves of TOKEM-320Y and TOKEM-400 resins are shown in Fig. 3.

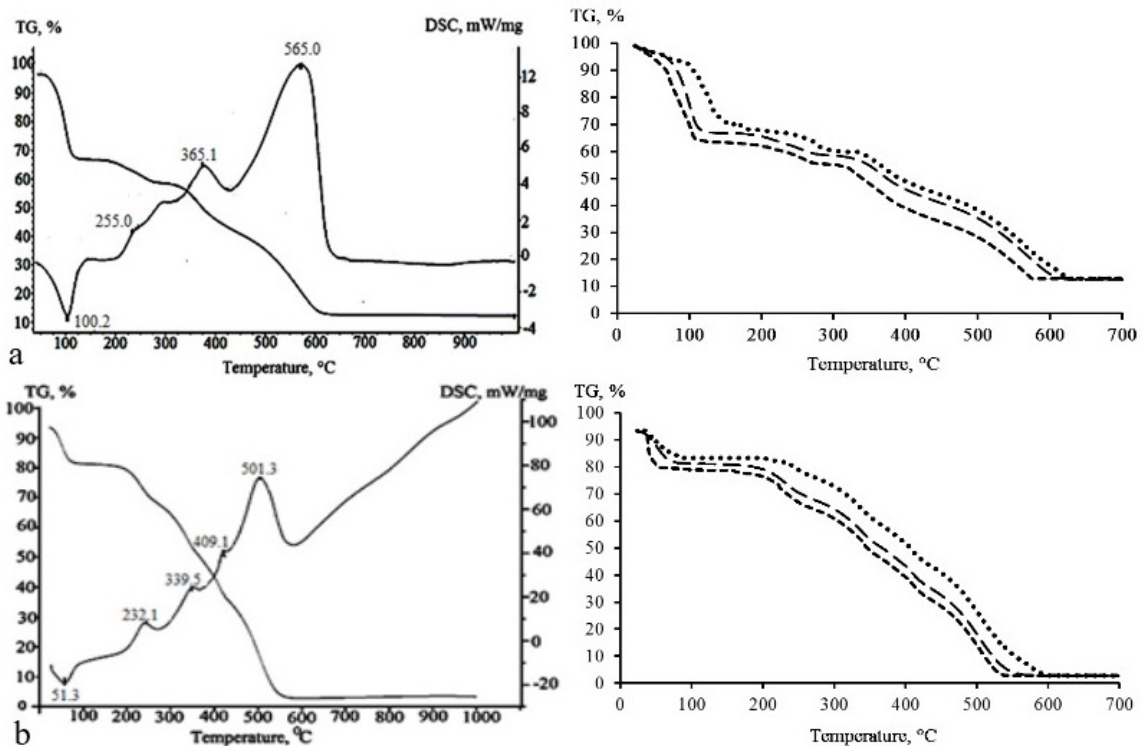


FIG. 3. Thermograms and TG-curves of degradation of resins (a) TOKEM-320Y, (b) TOKEM-400; at heating rates 7(---), 10(- - -), 12(····) deg min⁻¹

The shape of the thermograms suggests that TOKEM-320Y underwent four-step thermal decomposition and TOKEM-400 underwent five-step thermal decomposition. The peak temperatures T_{max} of each step with different heating rates are shown in Table 2. Kinetic parameters of thermal decomposition of resins by modified Kissinger

and Metzger-Horowitz methods have been determined. Kissinger plots were done using the data for T_{max} at various heating rates (Table 2). They are shown in Fig. 4.

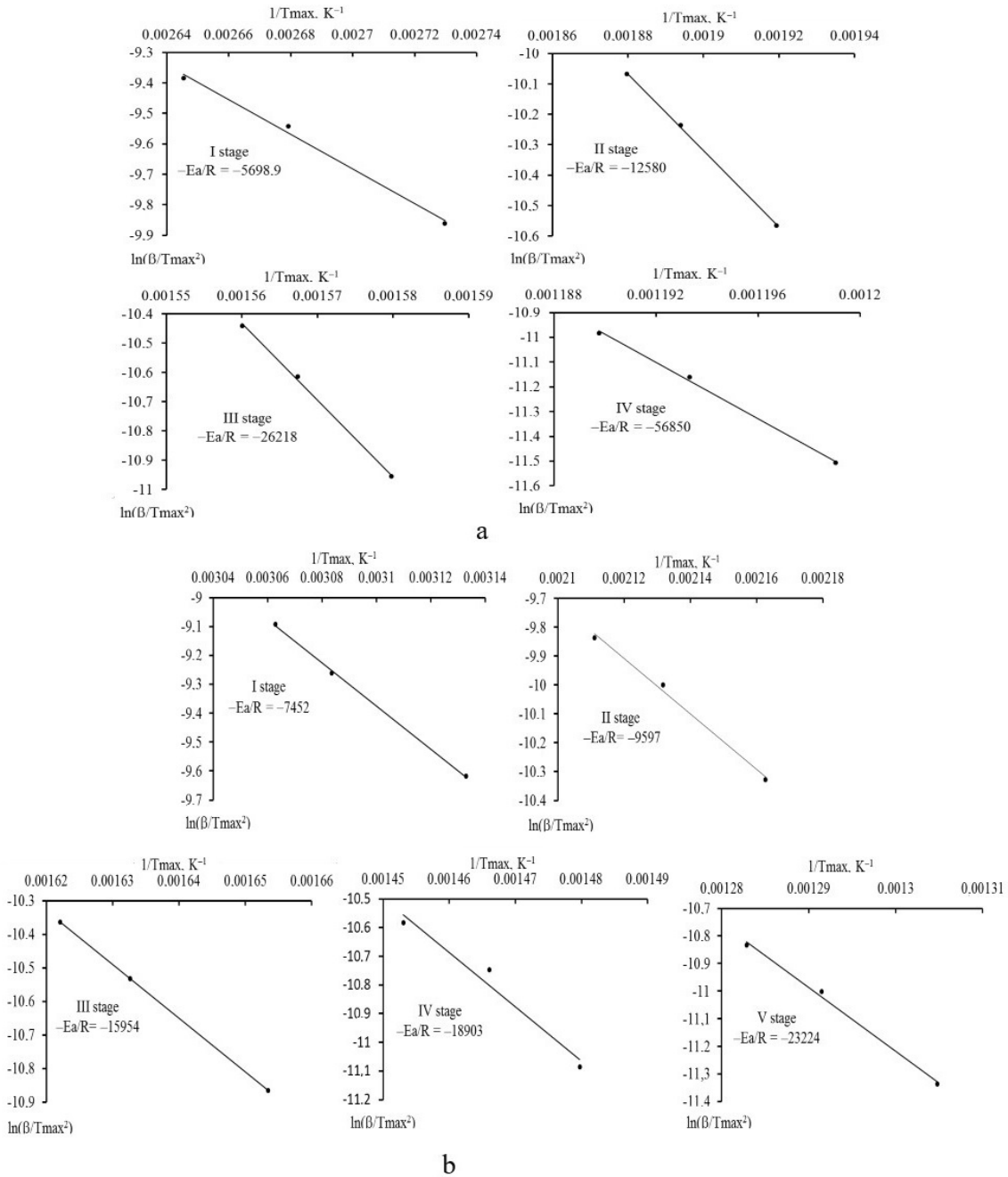


FIG. 4. Kissinger plots for the thermal decomposition of (a) TOKEM-320Y and (b) TOKEM-400 resins

The Metzger-Horowitz plots (Fig. 5) were performed for the thermograms of the TOKEM-320Y and TOKEM-400 decomposition at a rate of 10 deg min^{-1} using the values of the reaction order (n) which were determined by the Kissinger and calculated by the Metzger-Horowitz methods. The reaction order obtained by the Kissinger method was used to determine the activation energy by the Metzger-Horowitz method, since in this method there is an error in the determination of $(1 - \alpha)_{T_{\text{max}}}$, which may lead to an incorrect value of n . However, the value of n for all stages of thermal decomposition of the resins could not be determined by the Kissinger method since some lines on the DSC (differential scanning calorimetry) curve have no clearly defined basis: II stage for the TOKEM-320Y; III and IV

TABLE 2. The peak temperatures T_{\max} of each step with different heating rates

Heating rate (β), °/min	Stage 1	Stage 2	Stage 3	Stage 4	Stage 5
	T_{\max} , °C				
	TOKEM-320Y/TOKEM-400				
7	95.3 / 46.2	248.1 / 225.4	360.4 / 331.8	561.1 / 402.8	- / 493.4
10	100.2 / 51.3	255.0 / 232.1	365.1 / 339.5	565.0 / 409.1	- / 501.3
12	112.0 / 53.5	259.3 / 236.7	368.2 / 343.5	567.5 / 415.2	- / 506.5

TABLE 3. Kinetic parameters of the decomposition of TOKEM-320Y and TOKEM-400 resins

TOKEM-320Y					
Method / Stage	I	II	III	IV	V
	25–160 °C	160–325 °C	325–445 °C	445–660 °C	
Ea, kJ mol ⁻¹					
Kissinger	47	105	218	473	no stage
Metzger-Horowitz	73/0.9	81/0.9	-	138/0.9	no stage
Metzger-Horowitz (n Kissinger)	69/0.9	-	168/1.4	115/0.6	no stage
TOKEM-400					
Method / Stage	I	II	III	IV	V
	25–100 °C	100–275 °C	275–365 °C	365–450 °C	450–600 °C
Ea, kJ mol ⁻¹					
Kissinger	62	80	133	157	193
Metzger-Horowitz	22/2.8	78/2.1	128/0.8	103/2.5	131/2.8
Metzger-Horowitz (n Kissinger)	63/1.0	76/2.0	-	-	80/1.2

stages for the TOKEM-400. The limitation of the applicability of the Metzger-Horowitz method does not allow us to determine the reaction order of the third stage of the TOKEM-320Y decomposition.

The kinetic parameters of each stage of thermal decomposition of the resins are presented in Table 3.

The activation energies for the first stage of the decomposition of the TOKEM-320Y and TOKEM-400 resins with endothermic effects as well as the mass spectra (Fig. 6) of their decomposition products suggest that at this stage the most mobile water molecules adsorbed on the resins were removed. Also, water molecules formed as a result of the destruction of weakly basic anion exchangers in the functional group were removed.

The Shatava method (Fig. 7) shows that the dehydration rate of resins is described by the Avrami kinetic equation $-\ln(1-\alpha) = k\tau$ and corresponds to the process of diffusion of water molecules through a layer of a solid phase with random nucleation and their growth. The activation energies of the second stage decomposition of the resins indicate chemical destruction of the anion-exchange resins matrix, which is accompanied with exothermic effects. As can be seen from the Fig. 6, at this stage, $C_3H_7^+$, $C_3H_4^+$, CH_3N^+ hydrocarbon fragments with mass numbers $m/z=43$, $m/z=40$, $m/z=29$ respectively were found in the gas phase from both resins.

In addition, the presence of CO ($m/z=28$) in the mass spectra of resins in the temperature range of the second stage was also observed, which indicates the oxidation of hydrocarbon structures. The decomposition rate of the TOKEM-320Y resin polymer matrix can be described by the equation with the maximum coefficient in the correlation

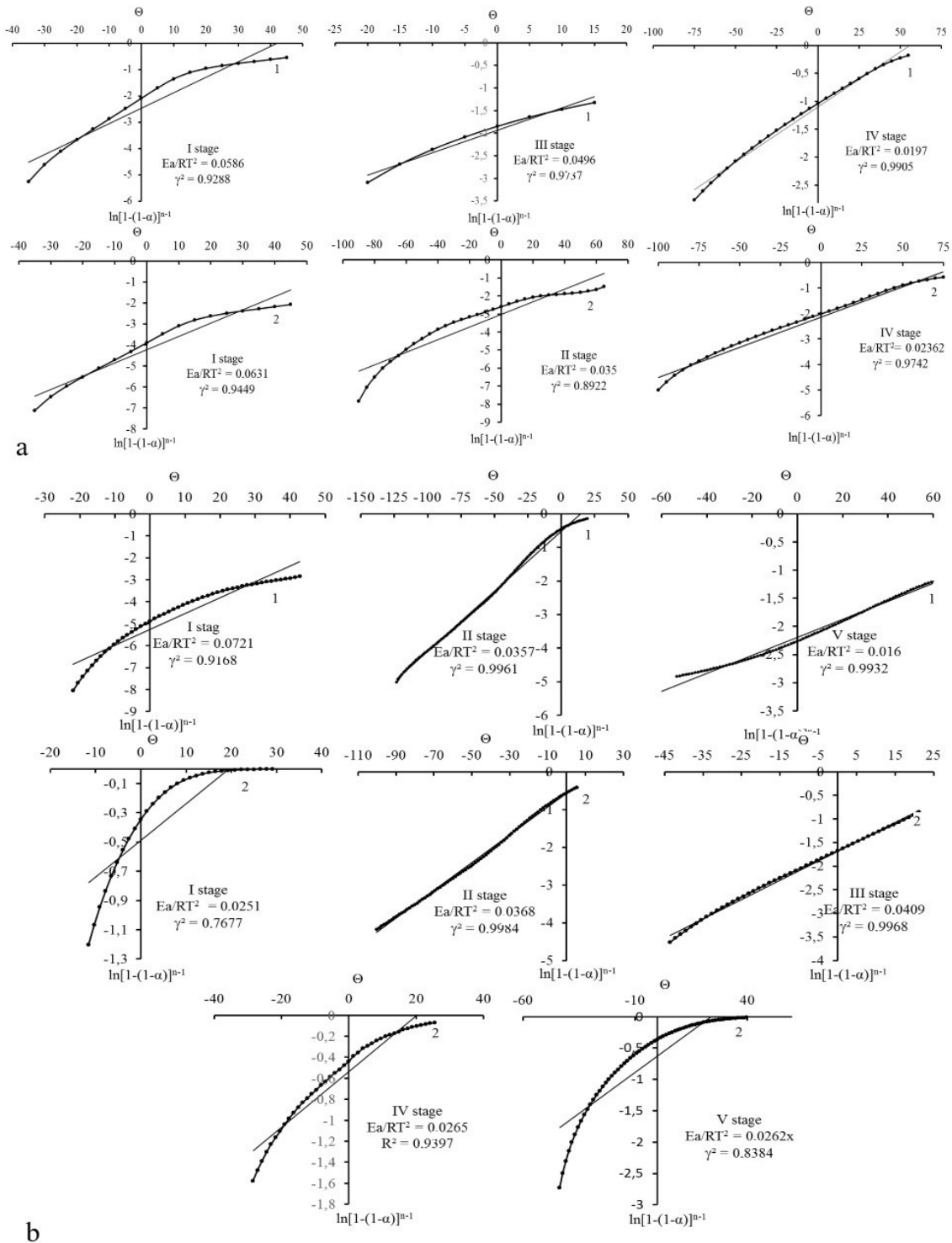


FIG. 5. Metzger-Horowitz plots for the decomposition of (a) TOKEM-320Y and (b) TOKEM-400 (reaction order (n) determined by the Kissinger (curves 1) and the Metzger-Horowitz (curves 2) methods)

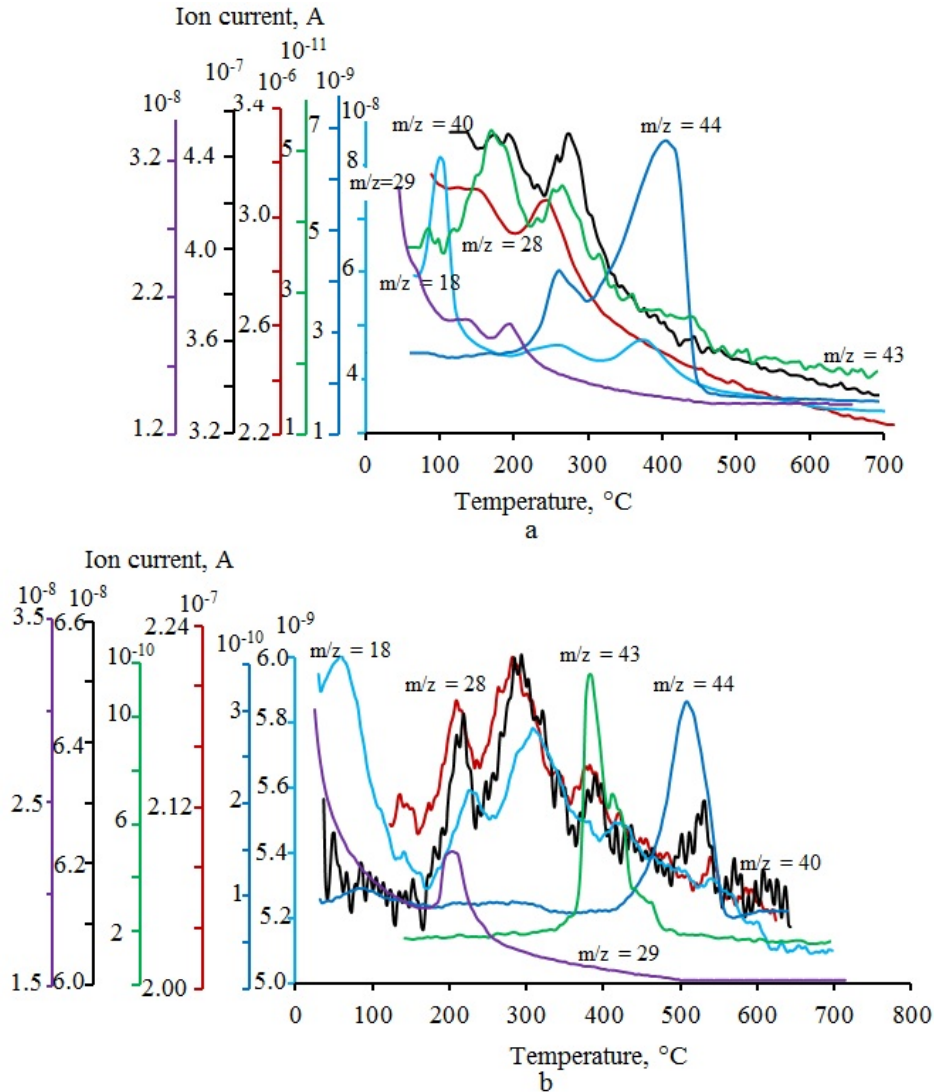


FIG. 6. Mass-spectrometric data for degradation products of the (a) TOKEM-320Y and (b) TOKEM-400 resins

coordinates of the linearity of the function $\log(g(\alpha))$ from $\frac{1}{T} 1 - (1 - \alpha)^{\frac{1}{2}} = k\tau$ which corresponds to the description of the reaction at the phase boundary of cylindrical symmetry. The decomposition of the TOKEM-400 resin polymer matrix is limited by a process that can be described using the Avrami equation (as well as in the first step. See Fig. 5). Random nucleation is a limiting stage. The polymer matrix of the TOKEM-400 resin continues to decompose in the third stage as well. The rate of its decomposition cannot be described by the Shatava method because the kinetic equations of different mechanisms of heterogeneous processes in coordinates $[\log(g(\alpha))] - \left[\frac{1}{T}\right]$ have linear character with correlation coefficients $R = 0.995-0.999$. The rate of decomposition of the TOKEM-320Y resin polymer matrix is described by two equations for the third step: the Yander equation $(1 - (1 - \alpha)^{\frac{1}{3}})^2 = k\tau$ and the reaction equation at the phase boundary of spherical symmetry $1 - (1 - \alpha)^{\frac{1}{3}} = k\tau$. At the fourth stage, the TOKEM-320Y anion exchange resin burns out with the formation of CO_2 and H_2O (Fig. 6) in the temperature range from 450 to 660°C. The limiting stage is described by the Avrami equation $-\ln(1 - \alpha) = k\tau$ (Fig. 7).

3.2. Thermal analysis of TOKEM-320Y and TOKEM-400 resins with $\text{Mo}_7\text{O}_{24}^{6-}$ ions and treated with the TBT-TEOS sol

Thermograms of the decomposition of TOKEM-320Y and TOKEM-400 resins loaded with $\text{Mo}_7\text{O}_{24}^{6-}$ ions and treated with the TBT-TEOS sol are presented in Fig. 8. The one endothermic and four exothermic peaks (Fig. 8b)

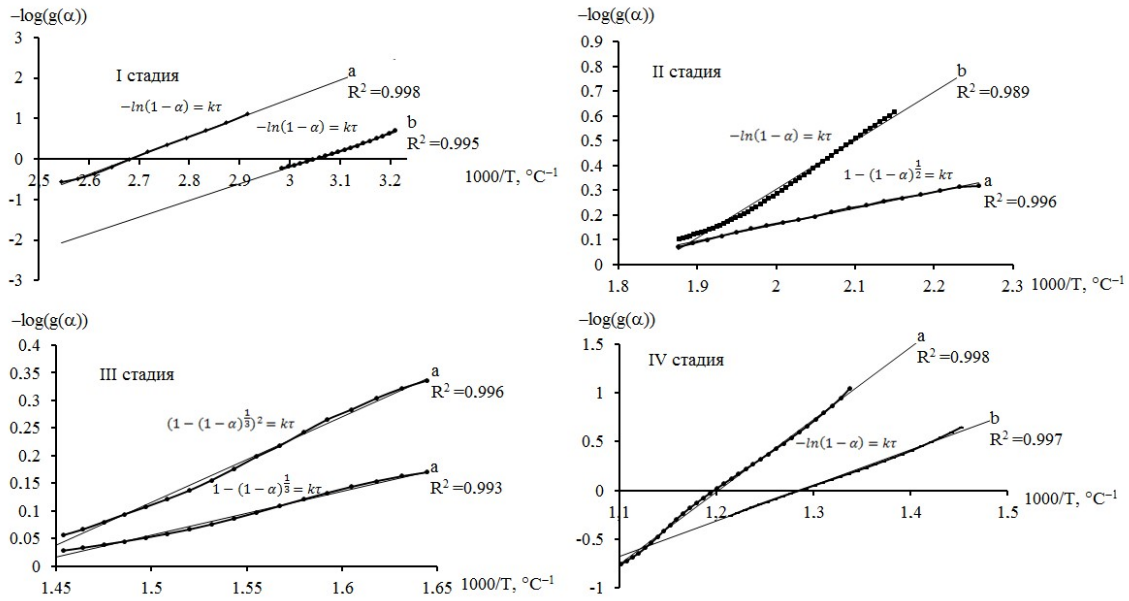


FIG. 7. The linearity of the function $\log(g(\alpha))$ of $1000/T$ for decomposition of (a) TOKEM-320Y and (b) TOKEM-400 resins

corresponding to the four stages of decomposition are observed on the thermogram of the decomposition of TOKEM-400 resin with $\text{Mo}_7\text{O}_{24}^{6-}$ ions and TBT-TEOS sol as well as on the thermogram of the decomposition of TOKEM-400 resin. Two high-temperature exothermic peaks with maxima at 485.1°C and 564.6°C , respectively, are observed in the fourth stage ($450\text{--}600^\circ\text{C}$). Therefore in this temperature range, parallel decomposition reactions are observed, the total activation energy of which is 193 kJ/mol and the reaction order was 1.1 (Horowitz-Metzger method); 156 kJ/mol and 0.8 (Kissinger method). Mass spectra indicate that these reactions were reactions of the burning of hydrocarbon residues with the formation of CO ($m/z = 28$), CO_2 ($m/z = 44$) and H_2O ($m/z = 18$) (Fig. 6b). It is known, that ammonium paramolybdate decomposes in three stages, which are accompanied by endothermic effects [31]. The formation of MoO_3 began in the third step above 290°C . The activation energy of this stage is 150 kJ/mol and the reaction order is ~ 1 . The decomposition of paramolybdate ion on the anion exchange resin cannot be established from the thermogram. The total process in the temperature range ($162\text{--}360^\circ\text{C}$, step two), where, according to the literature the formation of molybdenum oxide begins, is accompanied by an exothermic peak and is characterized by an activation energy of 65 kJ/mol with the reaction order 1.1 (Horowitz-Metzger method); 74 kJ/mol and 0.8 (Kissinger method). In this temperature range, the formation of H_2O ($m/z = 18$), CO ($m/z = 28$) and hydrocarbon residues with ($m/z = 40$) were observed in the gas phase. The thermogram of the TBT-TEOS/ $\text{Mo}_7\text{O}_{24}^{6-}$ (320Y) decomposition (Fig. 8a) indicates three stages, which were accompanied by one endothermic effect with a maximum of 93.8°C and exothermic effects that cannot be separated.

The Shatava method is not applicable to determine a suitable kinetic equation that would describe each step of the thermolysis of TOKEM-400 and TOKEM-320Y resins loaded with $\text{Mo}_7\text{O}_{24}^{6-}$ ions and treated with the TBT-TEOS sol because the kinetic equations of different mechanisms of heterogeneous processes in coordinates $[\lg(g\alpha)] - \left[\frac{1}{T}\right]$ have linear character with correlation coefficients $R = 0.995\text{--}0.999$. The decomposition temperature, at which the thermolysis of the TBT-TEOS/ $\text{Mo}_7\text{O}_{24}^{6-}$ (320Y) sample ends, is $\approx 500^\circ\text{C}$ and for the TBT-TEOS/ $\text{Mo}_7\text{O}_{24}^{6-}$ (400) sample is $\approx 600^\circ\text{C}$.

3.3. Phase composition, structure and surface morphology of oxide composites $\text{MoO}_3/\text{TiO}_2\text{-SiO}_2$

Phase compositions of the $\text{MoO}_3/\text{TiO}_2\text{-SiO}_2$ (320Y) and $\text{MoO}_3/\text{TiO}_2\text{-SiO}_2$ (400) composites obtained at 600°C were installed based on the results of XRD analysis. XRD patterns of the samples were identical. The XRD (Fig. 9) and refinement of the crystal structure by the Rietveld method indicate that the oxide composites are a mixture consisting of the main component of orthorhombic $\alpha\text{-MoO}_3$ and an admixture of TiO_2 with an anatase structure. The diffraction lines of the samples belong to orthorhombic $\alpha\text{-MoO}_3$ with the unit cell parameters $a = 1.387$, $b = 0.370$ and $c = 0.396\text{ nm}$. Based on the atomic coordinates, the structure of $\alpha\text{-MoO}_3$ was visualized using the VESTA

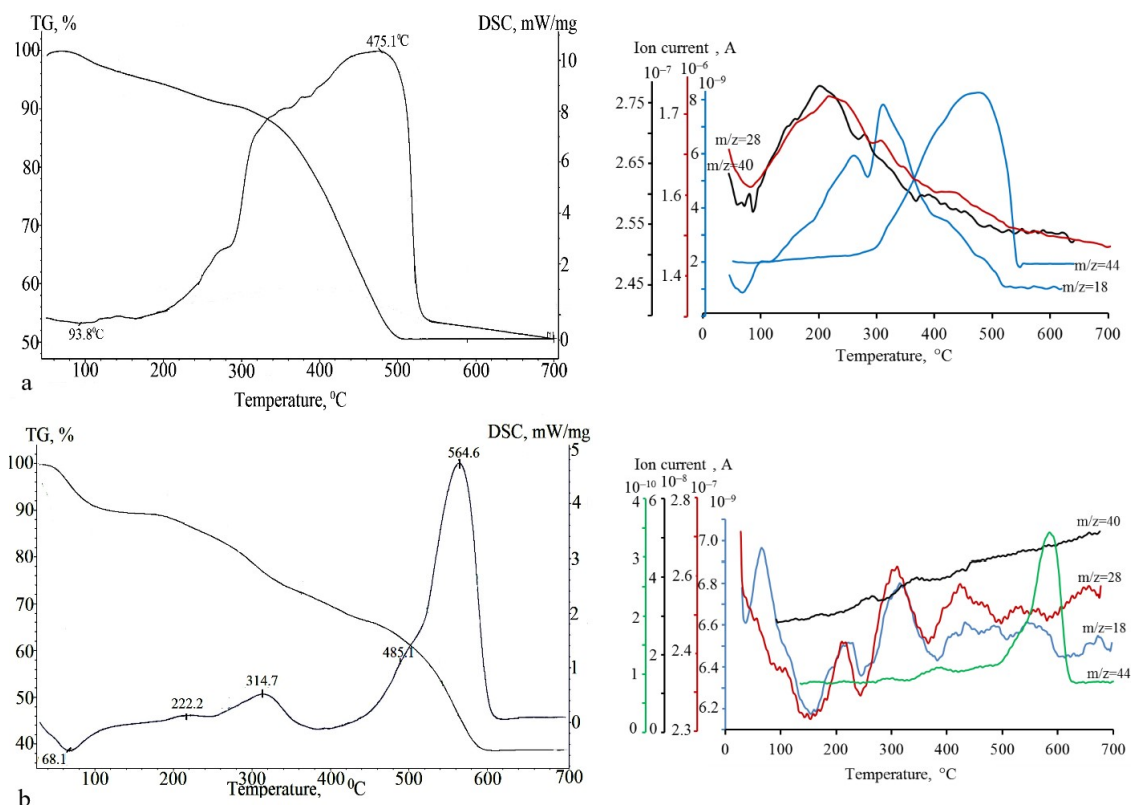


FIG. 8. Thermograms ($\beta = 10$ °C/min) and mass-spectrometric data for degradation products of (a) TBT-TEOS/Mo₇O₂₄⁶⁻ (320Y) and (b) TBT-TEOS/Mo₇O₂₄⁶⁻ (400) samples

program (Fig. 10). The samples obtained from different anion-exchange resins differ only in the grain size, which was estimated from the value of the coherent scattering region. The use of TOKEM-320Y resin makes it possible to obtain nanostructured composites with an average grain size of 25.6 nm, which form an agglomerate up to 7 μ m. The use of TOKEM-400 resin leads to the formation of composite grains with an average size of 55.5 nm, the grains of which form sintered agglomerates up to 150 μ m.

The structural characteristics are in good agreement with the literature data [37]. The presence of silicon oxide in the composites is confirmed by the results of MRSA (Fig. 11). X-ray emission spectra of MoO₃/TiO₂-SiO₂ (320Y) and MoO₃/TiO₂-SiO₂ (400) samples were identical. The spectrum contains characteristic lines corresponding to Mo, Ti, Si and O (Fig. 11). Consequently, the composites were a mixture of molybdenum and titanium crystalline oxides, as well as X-ray- amorphous silicon oxide.

SEM images show that the dense and non-destroyed spheres of the MoO₃/TiO₂-SiO₂ composites with diameters ranging from 0.3 to 0.5 μ m were formed from the precursors with TOKEM-320Y resin (Fig. 12a). As can be seen from the micrograph (the sphere we have broken), spheres are hollow inside.

The surfaces of the MoO₃/TiO₂-SiO₂ (320Y) spheres consists of many lamellar particles of various sizes and shapes. The particle size is from 0.5 to 3 microns. These particles are arranged irregularly and their appearance indicates the presence of several phases. The presence of several phases on the surface is also observed for MoO₃/TiO₂-SiO₂ (400) sample (Fig. 12b). As can be seen from the micrograph, dense spheres are not formed. Fig. 12b (the broken spheres) clearly shows that these spheres are hollow inside. The surface of the destroyed and non-destroyed spheres consists of sintered particles and has a large number of cracks. In addition, unlike the spheres obtained from precursors with TOKEM-320Y, these spheres are easily destroyed by mechanical action.

4. Conclusion

The nanostructured MoO₃/TiO₂-SiO₂ composites with hollow spherical form were obtained by the method of thermal decomposition of anion exchangers (TOKEM-320Y – porous structure, TOKEM-400 – gel structure) saturated with Mo₇O₂₄⁶⁻ ions and treated with the TBT-TEOS sol. The MoO₃/TiO₂-SiO₂ composite was a mixture of orthorhombic MoO₃, TiO₂ (anatase structure) and amorphous SiO₂. The presence of TiO₂ and SiO₂ in the composite

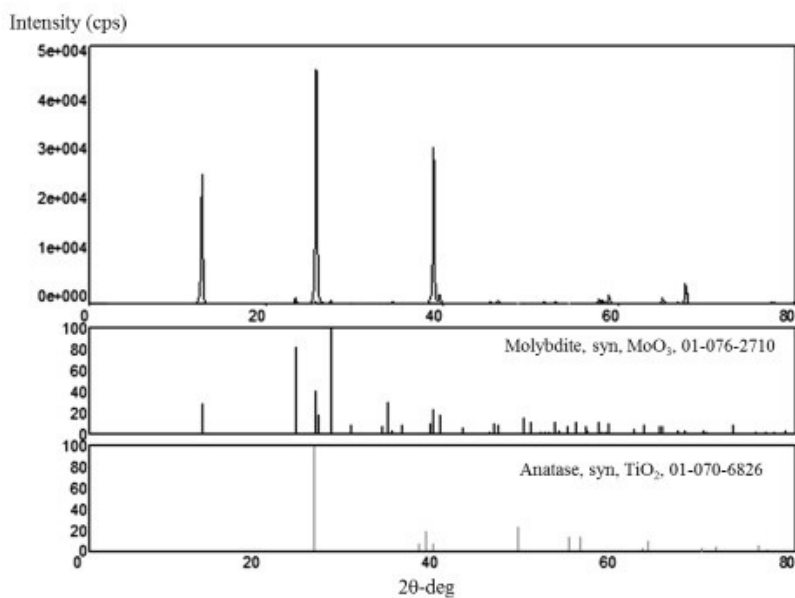


FIG. 9. X-ray diffraction patterns of prepared $\text{MoO}_3/\text{TiO}_2\text{-SiO}_2$ composites

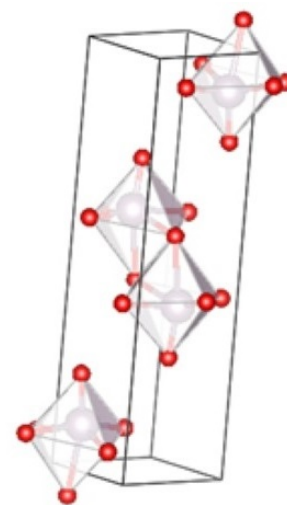


FIG. 10. Structure of $\alpha\text{-MoO}_3$ (Pnma)

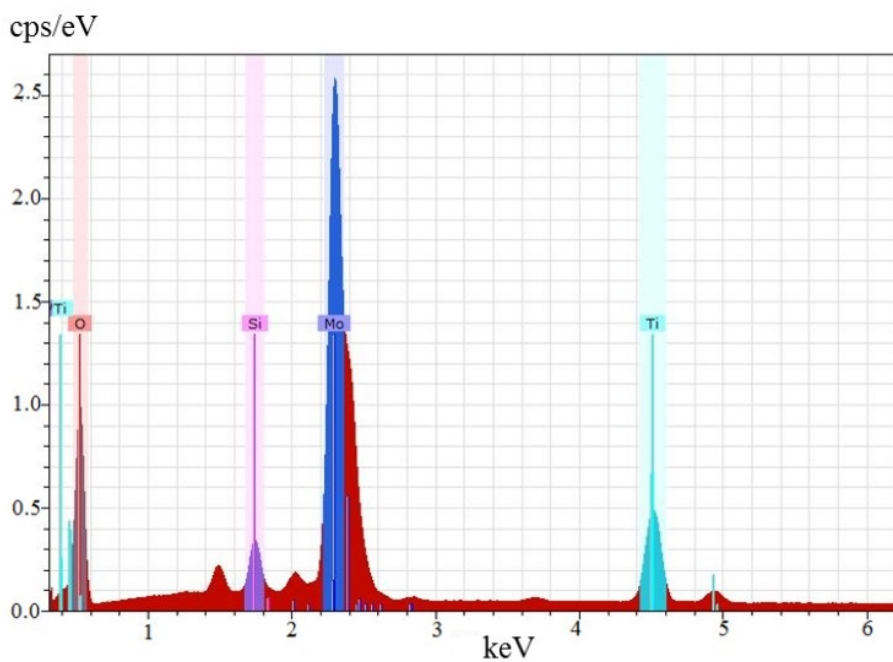


FIG. 11. X-ray emission spectrum of $\text{MoO}_3/\text{TiO}_2\text{-SiO}_2$ composites

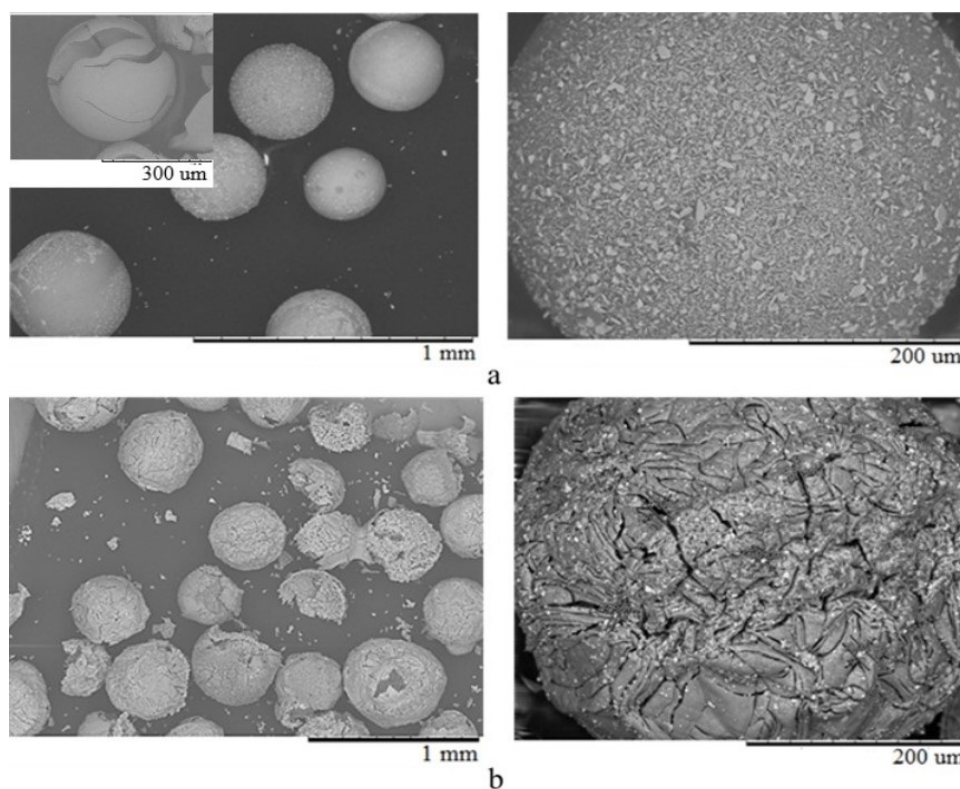


FIG. 12. Scanning electron micrographs of (a) $\text{MoO}_3/\text{TiO}_2\text{-SiO}_2$ (320Y) and (b) $\text{MoO}_3/\text{TiO}_2\text{-SiO}_2$ (400) composites

did not affect the MoO_3 structure. The decomposition kinetics of TOKEM-320Y and TOKEM-400 anion exchangers affected the surface morphology and strength of the spherical $\text{MoO}_3/\text{TiO}_2\text{-SiO}_2$ composites. Reactions and diffusive processes at the interface of cylindrical and spherical symmetries, where the velocity of the reaction boundary is the same in all directions contribute to the formation of dense spherical agglomerates. The decomposition reactions of the anion-exchange resin, accompanied with random nucleation, resulted in spherical agglomerates that had cracks on the surface. The activation energy of each stage of thermal destruction of anion exchange resins obtained by the Kissinger method slightly differed from the values of activation energies obtained by the Metzger-Horowitz method. However, there is a pattern, i.e., an increase in the decomposition temperature of resins leads to an increase in activation energy. The discrepancy between the reaction order by Shatava method and that by the Kissinger and Metzger-Horowitz methods proved the low sensitivity of the latter method in multistage processes. The reactions and diffusion proceeded at the interface of cylindrical and spherical symmetries, where the velocity of the reaction boundary was the same in all directions contributed to the formation of dense spherical agglomerates.

Acknowledgements

This work was performed within the framework of the government assignment of the Ministry of Science and Higher Education of the Russian Federation, project no. 0721-2020-0037.

References

- [1] Li W.Z., Qin C.G., Xiao W.M., Sheng J. Preparation of hollow layered MoO_3 microspheres through a resin template approach. *J. Solid State Chem.*, 2005, **178**, P. 390–394.
- [2] Vladimirova E.V., Gyrdasova O.I., Dmitriev A.V. Synthesis of nanostructured hollow microspheres of vanadium (III, V) oxides. *Nanosystems: physics, chemistry, mathematics*, 2020, **11**(5), P. 572–577.
- [3] Wang M.L., Wang C.H., Wang W. Porous macrobeads composed of metal oxide nanocrystallites and with percolated porosity. *J. Mater. Chem.*, 2007, **17**, P. 2133–2138.
- [4] Wang M.L., Wang, C.H. Wang W. Preparation of porous $\text{ZrO}_2/\text{Al}_2\text{O}_3$ macrobeads from ion-exchange resin templates. *J. Mater. Sci.*, 2011, **46**, P. 1220–1227.
- [5] Kuznetsova S.A., Brichkov A.S., Lisitsa K.V., Shamsutdinova A.N., Kozik V.V. Preparation and Properties of $\text{MoO}_3\text{-TiO}_2\text{-SiO}_2$ Composites with Spherical Shape of Agglomerates. *Russ. J. Appl. Chem.*, 2019, **92**, P. 171–180.

- [6] Rogacheva A., Shamsutdinova A., Brichkov A., Larina T., Paukshtis E., Kozik V. Synthesis and Properties of Spherical Catalysts TiO₂-SiO₂/M_xO_y (M=Co and Cr). *AIP Conf. Proc.*, 2017, **1899**, P. 020007.
- [7] Rogacheva A.O., Buzaev A.A., Brichkov A.S., Khalipova O.S., Klestov S.A., Paukshtis E.A., Kozik V.V. Catalytically active composite material based on TiO₂/Cr₂O₃ hollow spherical particles. *Kinet. Catal.*, 2019, **60**(4), P. 484–489.
- [8] Chandra P., Doke D.S., Umbarkara S.B., Birada A.V. One-pot synthesis of ultrasmall MoO₃ nanoparticles supported on SiO₂, TiO₂, and ZrO₂ nanospheres: an efficient epoxidation catalyst. *J. Mater. Chem. A.*, **2**(44), 2014, P. 219060–19066.
- [9] Ion exchange method for preparing metal oxide microspheres. Patent. 3438749 USA, Lonadier F.D., Brown W.B., Fushimi F.C., Silver G.L., p. 3.
- [10] Apblett A.W., Kuriyavar S.I., Kiran B.P. Preparation of micron-sized spherical porous iron oxide particles. *J. Mater. Chem.*, 2003, **13**, P. 983–985.
- [11] Castro I.A.D., Datta R.S., Ou J.Z., Gomez A.C., Sriram S., Daeneke T., Zadeh K.K. Molybdenum oxides from fundamentals to functionality. *Adv. Mater.*, 2017, **29**, P. 1701619.
- [12] Santos-Beltrán M., Paraguay-Delgado F., García R., Antúnez-Flores W., Ornelas-Gutiérrez C., Beltrán A.S. Fast methylene blue removal by MoO₃ nanoparticles. *J. Mater. Sci: Mater. Electron.*, 2017, **28**, P. 2935–2948.
- [13] Liu K., Huang X., Pidko E.A., Emiel J.M. MoO₃-TiO₂ synergy in oxidative dehydrogenation of lactic acid to pyruvic acid, *Green Chem.*, 2017, **19**, P. 3014–3022.
- [14] Li C.J., Tseng C.M., Lai S.N., Yang C.R., Hung W.H. Photocatalytic activities enhanced by Au-plasmonic nanoparticles on TiO₂ nanotube photoelectrode coated with MoO₃. *Nanoscale Res. Lett.*, 2017, **12**, P. 560–566.
- [15] Wang X., Cui W., Chen M., Xu Q. Supercritical CO₂-assisted phase transformation from orthorhombic to hexagonal MoO₃. *Mater. Lett.*, 2017, **201**, P. 129–132.
- [16] Bian L., Wang S.P., Ma X.B. The effect of catalyst preparation on the activity of MoO₃-SiO₂ catalyst in transesterification of diethyl oxalate. *Kinet. Catal.*, 2014, **55**, P. 763–769.
- [17] Kozik V.V., Brichkov A.S., Shamsutdinova A.N., Paukshtis E.A., Brichkova V.Y., Parmon V.N., Ivanov V.K. Stabilization of TiO₂-Co₃O₄ thin films on a glass fiber material by introduction of silica into the matrix. *Dokl. Phys. Chem.*, 2016, **470**, P. 154–157.
- [18] Li Y., Yu H., Huang X., Wu Z., Xu H. Improved performance for polymer solar cells using CTAB-modified MoO₃ as an anode buffer layer. *Sol. Energy Mater. Sol. Cells*, 2017, **171**, P. 72–84.
- [19] Kociotek-Balawejder E., Stanisławska E., Mucha I. Freeze dried and thermally dried anion exchanger doped with iron(III)(hydr)oxide – Thermogravimetric studies. *Thermochim. Acta*, 2019, **680**, P. 178359–178370.
- [20] Kalistratova V.V., Rodin A.V., Emel'yanov A.S., Vidanov V.L., Milyutin V.V., Belova E.V., Shmidt O.V., Myasoedov B.F. Kinetics of thermal degradation of VP-1AP anion-exchange resin in the nitrate form. *Radiochem.*, 2018, **60**, P. 287–293.
- [21] Ostroushko A.A., Mogil'nikov Yu.V., Ostroushko I.P. Synthesis of molybdenum- and vanadium-containing mixed oxides in polymer-salt systems. *Inorganic Materials*, 2000, **36**(12), P. 1256–1263.
- [22] Ostroushko A.A., Mogil'nikov Yu.V., Popov K.A. Thermal destruction of polymer-salt compositions containing d-metals in the form of oxygen-bearing anions. *Inorganic Materials*, 2000, **36**(6), P. 603–611.
- [23] Bogdanov S.G., Ostroushko A.A., Valiev E.Z., Pirogov A.N., Teplykh A.E. Effect of acidity of polymer-salt composition on the formation mechanism of the tungsten and molybdenum oxide particles. *J. of Surf. Investig.: X-Ray, Synchrotron and Neutron Techniques*, 2011, **5**(4), P. 21–32.
- [24] Shamsutdinova A.N., Brichkov A.S., Paukshtis E.A., Larina T.V., Cherepanova S.V., Glazneva T.S., Kozik V.V. Composite TiO₂/fiberglass catalyst: Synthesis and characterization. *Catal. Commun.*, 2017, **89**, P. 64–68.
- [25] Brichkov A.S., Shamsutdinova A.N., Khalipova O.S., Rogacheva A.O., Larina T.V., Cherepanova S.V., Glazneva T.S., Paukshtis E.A., Buzaev A.A., Kozik V.V., Chen Y.-W. Preparation of a fiberglass-supported Ni-Si-Ti oxide catalyst for oxidation of hydrocarbons: effect of SiO₂. *J. Chem. Technol. Biotechnol.*, 2019, **94**, P. 3618–3624.
- [26] Leykin Y.A., Meychik N.R., Solovyov V.K. Acid-base equilibrium of polyamfolitov with pyridine and phosphate groups. *Russian J. Phys. Chem.*, 1978, **52**, P. 1420–1424.
- [27] Busev A.I. *Analytical Chemistry of Molybdenum*. Ann Arbor-Humphrey Science Publishers, Moscow, 1969, 253 p.
- [28] Kissinger H.E. Variation of peak temperature with heating rate in differential thermal analysis. *J. Res. Nat. Bur. Standards*, 1956, **57**, P. 217–221.
- [29] Kissinger H.E. Reaction kinetics in differential thermal analysis. *Anal. Chem.*, 1958, **29**, P. 1702–1706.
- [30] Zeng W., Zhou H., Chen Q., Chen X. Kinetics of thermal decomposition of synthetic gibbsite. *Transactions of Nonferrous Metals Society of China*, 1993, **3**(2), P. 41–44.
- [31] Yin Z., Li X., Chen Q. Study on the kinetics of the thermal decomposition of ammonium molybdates. *Thermochim. Acta.*, 2000, **352–353**, P. 107–110.
- [32] Gul S., Shah A.A., Bilal S. Calculation of activation energy of degradation of polyaniline-dodecylbenzene sulfonic acid salts via TGA. *J. Sci. Innovative Research*, 2013, **2**, P. 673–684.
- [33] Šatava V., Škvara Fr. Mechanism and kinetics of the decomposition of solids by a thermogravimetric method. *J. Am. Ceram. Soc.*, 1969, **52**, P. 591–595.
- [34] Bortolotti M., Lonardelli I. ReX. Cell: a user-friendly program for powder diffraction indexing. *J. Appl. Cryst.*, 2013, **46**, P. 259–261.
- [35] Boultif A., Louër D. Powder pattern indexing with the dichotomy method. *J. Appl. Cryst.*, 2004, **37**, P. 724–731.
- [36] Momma K., Izumi F. VESTA 3 for three-dimensional visualization of crystal, volumetric and morphology data. *J. Appl. Crystallogr.*, 2011, **44**, P. 1272–1276.
- [37] Crystallography Open Database: www.crystallography.net.